Polyhedron 176 (2020) 114182

Contents lists available at ScienceDirect

Polyhedron

journal homepage: www.elsevier.com/locate/poly

Molecular spin frustration in mixed-chelate Fe_5 and Fe_6 oxo clusters with high ground state spin values ☆

Alok P. Singh [a], Rajendra P. Joshi [b], Khalil A. Abboud [a], Juan E. Peralta [b], George Christou [a,*]

[a] Department of Chemistry, University of Florida, Gainesville, FL 32611-7200, USA
[b] Department of Physics and Science of Advanced Materials, Central Michigan University, Mount Pleasant, MI 48859, USA

ARTICLE INFO

Article history:
Received 31 August 2019
Accepted 15 October 2019
Available online 23 October 2019

Keywords:
Iron
Cluster
Crystal structure
Magnetic properties
DFT

ABSTRACT

The synthesis, structures, and magnetic properties are reported of three new polynuclear Fe^{III} complexes containing the anions of picolinic acid (picH) and triethanolamine ($teaH_3$) as chelates. The complexes $[Fe_6O_2(OH)_2(O_2CR)_4(pic)_4(teaH)_2]$ (R = Me (**1**), Ph (**2**)) and $[Fe_5O_2(O_2CBu^t)_4(pic)_3(teaH)_2]$ (**3**) were obtained from the reaction of $[Fe_3O(O_2CR)_6(H_2O)_3](NO_3)$ (R = Me, Ph, Bu^t) with picH and $teaH_3$ in a 1:2:1 ratio in MeCN. The core of **1** and **2** consists of an $[Fe_4(\mu_3\text{-}O)_2]^{8+}$ 'planar-butterfly' unit to which is attached an Fe atom on either side by bridging O atoms. The core of **3** consists of an $[Fe_5(\mu_3\text{-}O)_2]^{11+}$ unit comprising two near-perpendicular vertex-sharing $[Fe_3(\mu_3\text{-}O)]^{7+}$ triangular units. Variable-temperature (T) and -field (H) solid-state dc and ac magnetization (M) studies in the 5.0–300 K temperature range revealed that **1** and **2** have an $S = 5$ ground state spin whereas **3** has an $S = {}^5/_2$ ground state. J_{ij} exchange couplings were calculated by DFT and a magnetostructural correlation (MSC) for polynuclear Fe^{III}/O complexes. This allowed rationalization of the observed ground states from the analysis of the spin frustration effects operative, and provided good input values for fits of the experimental $\chi_M T$ vs T data to obtain the J_{ij} values.

1. Introduction

The chemistry of iron(III)-oxo complexes continues to attract considerable research interest owing to its significance and relevance to a wide range of areas including bioinorganic chemistry, molecular magnetism, and materials science. A large number of Fe^{III}/O complexes of various nuclearities have consequently been synthesized over the years – from dinuclear ones to model the Fe_2 sites of biomolecules such as methane monooxygenase [1–6], hemerythrin [7–9], ribonucleotide reductase [1,2,10], and others [11–13], through to higher nuclearity clusters useful for studies of interesting magnetic properties and spin frustration effects [14–17], and even to model intermediate stages in the growth of the giant Fe/O core of the iron storage protein ferritin [18–22], which comprises a highly symmetrical near-spherical shell of 24 polypeptide subunits and encapsulates up to 4500 Fe atoms [23–26].

In Fe^{III} chemistry, high nuclearity Fe/O^{2-} clusters are facilitated by the high charge-to-size ratio of Fe^{III}, which favors deprotonation of H_2O to form O^{2-} bridges [14,27,28]. This also leads to strong Fe^{III}_2 exchange coupling and, although this is essentially always antiferromagnetic (**AF**), certain Fe_x topologies can lead to spin frustration effects from competing exchange interactions, which can yield high spin ground states and even single-molecule magnets if sufficient magnetic anisotropy from a significant and negative zero-field splitting is present [14,29–35].

For the above reasons, there is continuing interest in developing new synthetic routes to Fe^{III}/O clusters. In the past, the use of various chelating and/or bridging ligands has led to many Fe^{III}/O core topologies and nuclearities up to Fe_{22} [14,32,36–39]. Most procedures employ two ligand types, such as carboxylates and a chelate, but the use of three or more ligand types is poorly explored. Therefore, we have been investigating combining carboxylates with two different types of chelates in a search for new Fe^{III}/O clusters, and describe in this report some recent results using picolinic acid (picH) and triethanolamine ($teaH_3$). Both picH and $teaH_3$ have separately yielded a variety of Fe/O clusters [40–48], but to our knowledge they have not been used together in Fe chemistry. We herein describe the syntheses, structures, and magnetochemical characterization of three new Fe^{III}/O clusters containing pic^- and $teaH^{2-}$.

☆ Dedicated to the founding in 2019 of the annual *Molecular Magnetism in North America* (MAGNA) workshop.

* Corresponding author.
E-mail address: christou@chem.ufl.edu (G. Christou).

https://doi.org/10.1016/j.poly.2019.114182
0277-5387/

2. Experimental

2.1. Syntheses

All preparations were performed under aerobic conditions using reagents and solvents as received, unless otherwise stated. $[Fe_3O(O_2CMe)_6(H_2O)_3](NO_3)$, $[Fe_3O(O_2CPh)_6(H_2O)_3](NO_3)$ and $[Fe_3O(O_2CBu^t)_6(H_2O)_3](NO_3)$ were prepared as reported previously [49].

2.1.1. $[Fe_6O_2(OH)_2(O_2CMe)_4(pic)_4(teaH)_2]$ (**1**)

To a stirred red solution of $[Fe_3O(O_2CMe)_6(H_2O)_3](NO_3)$ (0.32 g, 0.50 mmol) in MeCN (15 mL) was added picH (0.12 g, 1.0 mmol) followed by $teaH_3$ (0.07 g, 0.50 mmol). The mixture was stirred for one hour at room temperature and filtered to remove any undissolved solids. The red filtrate was allowed to concentrate at ambient temperature by slow evaporation over three days, during which time red crystals of **1**·4MeCN grew. These were collected by filtration, washed with Et_2O, and dried under vacuum; the yield was 34% with respect to Fe. *Anal.* Calc. (Found) for **1**·MeCN ($C_{46}H_{59}Fe_6N_7O_{26}$): C, 37.81 (37.99); H, 4.07 (4.27); N, 6.71 (6.72) %. Selected IR data (KBr, cm^{-1}): 3442 (br), 1699(w), 1599(m), 1553 (m), 1409(s), 1290(m), 1024 (w), 719(m), 675(w), 614(m), 481(m).

2.1.2. $[Fe_6O_2(OH)_2(O_2CPh)_4(pic)_4(teaH)_2]$ (**2**)

Complex **2** was prepared following the same procedure as for **1** but with $[Fe_3O(O_2CPh)_6(H_2O)_3](NO_3)$ (0.50 g, 0.50 mmol). The yield was 42% with respect to Fe. *Anal.* Calc. (Found) for **2**·MeCN ($C_{66}H_{67}Fe_6N_7O_{26}$): C, 46.13 (46.22); H, 3.99 (4.09); N, 5.71 (5.41) %. Selected IR data (KBr, cm^{-1}): 3450(br), 1672(m), 1655(m), 1591(m), 1539(s), 1474(w), 1405(s), 1290(m), 1069(w), 1044(w), 719(m), 645(m), 574(m), 459(m).

2.1.3. $[Fe_5O_2(O_2CBu^t)_4(pic)_3(teaH)_2]$ (**3**)

To a stirred orange-red solution of $[Fe_3O(O_2CBu^t)_6(H_2O)_3](NO_3)$ (0.45 g, 0.50 mmol) in MeCN (15 mL) was added picH (0.12 g, 1.0 mmol) followed by $teaH_3$ (0.07 g, 0.50 mmol). The dark brown mixture was stirred for one hour at room temperature and filtered to remove any undissolved solids. The filtrate was allowed to concentrate at ambient temperature by slow evaporation over 3 days, during which time black crystals of **3**·$^1/_2$$teaH_3$·2MeCN grew. These were collected by filtration, washed with Et_2O, and dried under vacuum; the yield was 37% with respect to Fe. *Anal.* Calc. (Found) for **3**·MeCN ($C_{52}H_{77}Fe_5N_6O_{22}$): 44.06 (44.32), 5.48 (5.88), 5.93 (5.64) %. Selected IR data (KBr, cm^{-1}): 3408(br), 2962(m), 1676 (w), 1638(s), 1601(m), 1557(s), 1422(m), 1374(m), 1096(m), 1046(m), 708(m), 676(m), 644(w), 603(w), 494(m), 437(m).

2.2. X-ray crystallography

X-ray data were collected at 100 K on a Bruker **DUO** diffractometer using Mo Kα radiation ($\lambda = 0.71073$ Å) and an APEXII CCD area detector. Raw data frames were read by program SAINT and integrated using 3D profiling algorithms. The resulting data were reduced to produce *hkl* reflections, and their intensities and estimated standard deviations. The data were corrected for Lorentz and polarization effects, and numerical absorption corrections were applied based on indexed and measured faces. The structures were solved and refined in *SHELXTL2014* using full-matrix least-squares cycles [50]. The non-H atoms were refined with anisotropic thermal parameters, and all the H atoms were placed in calculated, idealized positions and refined as riding on their parent atoms. The refinement was carried out by minimizing the wR_2 function using F^2 rather than F values. R_1 is calculated to provide a reference to the conventional R-value, but its function is not minimized. Unit cell data and structure refinement details are listed in Table 1.

For **1**·4MeCN, the asymmetric unit consists of a half Fe_6 cluster and four partial MeCN solvent molecules. For one MeCN, with N81, this is caused by disorder in the uncoordinated alcohol arm of a $teaH^{2-}$ ligand, which was refined in two parts and with the H atom of its –OH placed in a calculated position. The other MeCN molecules had their site occupancies fixed at 50%, 50%, and 25%. In the final cycle of refinement, 8179 reflections (of which 7400 are observed with $I > 2\sigma(I)$) were used to refine 415 parameters, and the resulting R_1, wR_2 and S (goodness of fit) were 5.89%, 16.17% and 1.101, respectively.

For **3**·$^1/_2$$teaH_3$·2MeCN, the asymmetric unit consists of a Fe_5 cluster, a half $teaH_3$ molecule, and two MeCN solvent molecules. The H atoms of the –OH groups of the lattice $teaH_3$ and ligated $teaH^{2-}$ groups were placed in idealized positions. In the final cycle of refinement, 16 285 reflections (of which 13 700 are observed with $I > 2\sigma(I)$) were used to refine 826 parameters and the resulting R_1, wR_2 and S (goodness of fit) were 4.09%, 10.67% and 1.043, respectively.

2.3. Physical measurements

Infrared spectra were recorded in the solid-state (KBr pellets) on a Thermo Scientific Nicolet iS5 FTIR spectrometer in the 400–4000 cm^{-1} range. Elemental analyses (C, H, N) were performed by Atlantic microlab in Norcross, Georgia, USA. Variable-temperature dc and ac magnetic susceptibility data were collected at the University of Florida using a Quantum Design MPMS-XL SQUID magnetometer equipped with a 7 T magnet and operating in the 1.8–300 K range. Samples were embedded in solid eicosane to prevent torquing. Pascal's constants were used to estimate the diamagnetic corrections [51], which were subtracted from the experimental susceptibility to give the molar paramagnetic susceptibility (χ_M).

2.4. DFT calculations

DFT calculations were performed using the hybrid version of the Perdew–Burke–Ernzerhof (PBEh) functional, which includes 25% of exact (Hartree–Fock type) exchange. This functional is known to perform well for magnetic exchange couplings [52–55],

Table 1
Crystallographic and structure refinement data for complexes **1** and **3**.

	1·4MeCN	**3**·½ $teaH_3$·2MeCN
Formula[a]	$C_{52}H_{68}Fe_6N_{10}O_{26}$	$C_{54}H_{80}Fe_5N_8O_{22}$
FW (g mol^{-1})[a]	1584.22	1472.48
Space group	$P2_1/n$	$P\bar{1}$
Unit cell dimensions		
a (Å)	14.6785(8)	13.5882(6)
b (Å)	11.9614(7)	13.8747(6)
c (Å)	20.7528(12)	21.632(1)
α (°)	90	80.314(1)
β (°)	102.187(1)	73.529(1)
γ (°)	90	65.256(1)
V (Å^3)	3561.6(4)	3546.1(3)
Z	2	2
T (K)	100(2)	100(2)
λ (Å)	0.71073	0.71073
D_{calc} (g cm^{-3})	1.510	1.436
μ (mm^{-1})	1.272	1.076
R_1[b,c]	0.0589	0.0409
wR_2[b,d]	0.1617	0.1067

[a] Including solvent molecules.
[b] $I > 2\sigma(I)$.
[c] $R_1 = \Sigma(||Fo| - |Fc||)/\Sigma|Fo|$.
[d] $wR_2 = [\Sigma[w(Fo^2 - Fc^2)^2]/\Sigma[w(Fo^2)^2]]^{1/2}$.

and for the particular case of oxo-bridged Fe··Fe couplings is expected to yield an RMS error of ~10% [56]. Pople's 6-311+G** basis was used for Fe atoms and 6-31G** for lighter elements [57]. All calculations included all the electrons and neglected scalar and spin-orbit relativistic effects. The structures of **1** and **3** for the DFT calculation were obtained from the cif's by cleaning extraneous atoms (lattice solvent and minor ligand disorder positions) and are provided as supporting material. To determine the exchange couplings, DFT calculations were carried out on the high-spin (all spins parallel) and all possible broken symmetry spin configurations: (i) 6 configurations with a single spin inversion, 15 with two inversions, and 10 with three inversions at the six Fe centers of **1** (32 configurations in total); and (ii) 10 single inversions and 10 double inversions for the five Fe centers of **3** (21 configurations in total). The resulting energies for the different magnetic configurations were used to perform an overdetermined linear fit of the Ising-type energy expression in Eq. (1), where <*ij*>

$$E(\{S\}) = -2\sum_{<ij>} J_{ij} S_i S_j + E_0 \quad (1)$$

stands for all *ij* pairs, giving 15 and 10 distinct couplings for **1** (Fe_6) and **3** (Fe_5), respectively. This strategy has been successfully used by others to extract exchange couplings in multicenter transition metal complexes [58]. As a way of testing the consistency of the fitting procedure, second-neighbor couplings were fixed at zero, and the fitted first-neighbor couplings were verified as being minimally affected. We have also verified that the atomic spin populations obtained are consistent with the expected broken spin symmetry configuration. All calculations were performed using an in-house version of the Gaussian 16 program that allows for simple spin inversion of magnetic centers to produce a reasonable initial guess for self-consistent calculations [59]. No symmetry was assumed at any point in the model or the DFT calculations. A threshold of 10^{-6} Ha = 0.2 cm^{-1} in the energy was used in all calculations.

Axial magnetic anisotropy (zero-field splitting) parameters, *D*, were calculated using the method of Pederson and Khanna [60] employing the PBE functional and the same basis set used for J_{ij} couplings, and taking the lowest energy broken-symmetry solution as the reference state. This approach has been shown to provide reasonable *D* parameters for a variety of large multinuclear transition metal complexes [61].

3. Results and discussion

3.1. Syntheses

A standard synthetic procedure to high-nuclearity Fe^{III} clusters that we and others have employed on numerous occasions in the past is the reaction of $[Fe_3O(O_2CR)_6L_3]^+$ (L = H_2O or similar) salts with potentially chelating ligands. The $[Fe_3O]^{7+}$ core serves as a useful building block to higher nuclearity species, and the chelates have the dual function of facilitating non-polymeric products and fostering high nuclearity products, especially for chelates containing alkoxide groups since these are excellent bridging groups. We thus chose to explore the reactions of $[Fe_3O(O_2CR)_6(H_2O)_3]^+$ salts with picH and $teaH_3$. Since it is also frequently seen that the product nuclearity and/or structure can vary with the carboxylate employed, such as in the reaction of $[Fe_3O(O_2CR)_6L_3]^+$ with dmemH ($Me_2NCH_2CH_2N(Me)CH_2CH_2OH$) [62], we also explored the effect in the present work of varying the carboxylate.

A number of reaction reagent ratios were explored before the following syntheses were developed. The reaction of $[Fe_3O(O_2CR)_6(H_2O)_3](NO_3)$ (R = Me or Ph) with picH and $teaH_3$ in a 1:2:1 ratio in MeCN gave red solutions from which were subsequently isolated $[Fe_6O_2(OH)_2(O_2CR)_4(pic)_4(teaH)_2]$ (R = Me (1) or Ph (2)). The reaction is summarized in Eq. (2).

$$2\left[Fe_3O(O_2CR)_6(H_2O)_3\right]^+ + 4picH + 2teaH_3 \rightarrow \left[Fe_6O_2(OH)_2(O_2CR)_4(pic)_4(teaH)_2\right] + 8RCO_2H + 4H_2O + 2H^+ \quad (2)$$

The similar formulas for **1** and **2** from the elemental analysis data, and their very similar IR spectra allowing for differences due to the carboxylates, suggest isostructural compounds except for the carboxylate identity, and this was also supported by their magnetic data (vide infra). For these reasons, the crystal structure of **2** was not pursued. In contrast, the same reaction using $[Fe_3O(O_2CBu^t)_6(H_2O)_3](NO_3)$ gave a dark brown solution from which isolated $[Fe_5O_2(O_2CBu^t)_4(pic)_3(teaH)_2]$, summarized in Eq. (3).

$$5\left[Fe_3O(O_2CR)_6(H_2O)_3\right]^+ + 9picH + 6teaH_3 \rightarrow 3\left[Fe_5O_2(O_2CR)_4(pic)_3(teaH)_2\right] + 18RCO_2H + 14H_2O + 5H^+ \quad (3)$$

Other reactions using small variations in the Fe^{III}/picH/$teaH_3$ ratios also gave compounds **1**, **2**, and **3** but in lower yields.

3.2. Description of structures

A stereoview of the centrosymmetric structure of **1** and its labeled core are shown in Fig. 1, and selected bond distances are shown in Table S1. The core consists of a $[Fe_4(\mu_3\text{-}O^{2-})_2]^{8+}$ 'planar-butterfly' unit on either side of which is attached an $[Fe(\mu\text{-}OH)(\mu\text{-}OR)_2]$ unit (Fe3/Fe3′) in a tripodal fashion, where RO

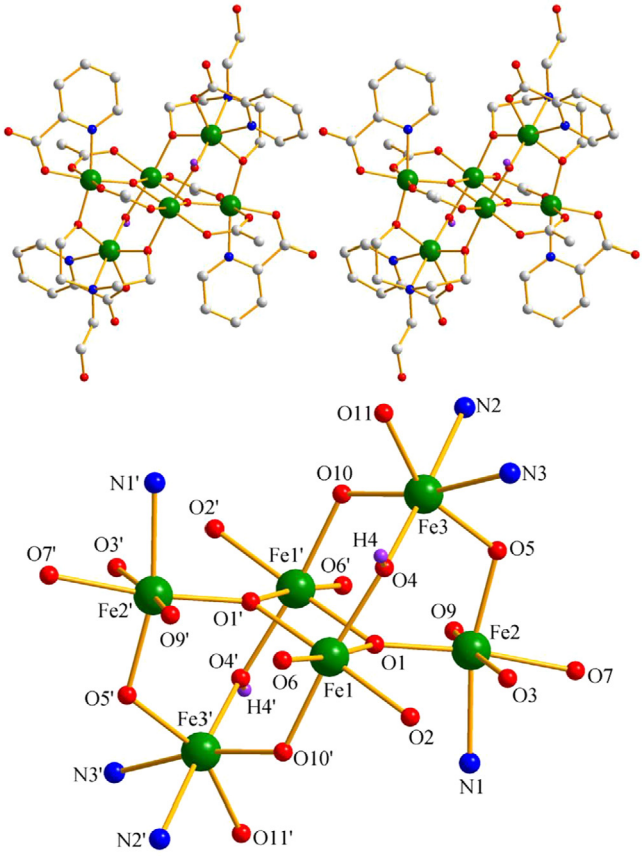

Fig. 1. A stereopair of the complete structure of complex **1**, and its labeled core; H atoms have been omitted for clarity except those on the μ-OH^- ion. Color code: Fe, green; O, red; N, blue; C, gray. (Color online.)

are alkoxide arms of $teaH^{2-}$ groups. All metals atoms are Fe^{III} with near-octahedral geometry [63]. The protonated μ-OH^- nature of O4 was confirmed by an O bond valence sum (BVS) calculation, which gave a value of 1.10 (Table S2). Peripheral ligation is provided by two N,O,O-chelating $teaH^{2-}$ groups also bridging to the butterfly unit as described (and with the protonated alcohol arm unbound), four acetate groups in their common *syn,syn* μ-bridging mode, and four N,O-chelating pic^- groups, one each on Fe2, Fe3, and their symmetry partners; the complete molecule has crystallographic C_i symmetry. It is interesting to note that the $[Fe_4O_2(O_2CR)_7(pic)_2]^-$ anion with a butterfly structure has been previously reported [42], so **1** can be considered as resulting from the replacement of some of its acetate groups on either side by the two $[Fe^{III}(\mu\text{-}OH)(\mu\text{-}OR)_2]$ units.

Each molecule of **1** is hydrogen-bonded to four neighboring molecules to give planar 2-D sheets, each contact involving an unbound $teaH^{2-}$ alcohol arm (O13) and an unbound O12 atom of the pic^- group (O13···O12 = 2.655(4) Å). Between the sheets lie the MeCN solvent molecules.

There are a large number of Fe_6 complexes in the literature, with a variety of topologies such as chair, twisted boat, parallel triangles, planar, octahedral, ladder-like, cyclic, etc. Previous compounds with some similarity to **1** nevertheless differ in the means of connection of additional Fe atoms to the Fe_4 butterfly unit and in the identity of the peripheral ligands [39,62,64–66].

A stereoview of the centrosymmetric structure of **3** and its labeled core are shown in Fig. 2, and selected bond distances are shown in Table S3. The core consists of an $[Fe_5(\mu_3\text{-}O)_2]^{11+}$ unit comprising two near-perpendicular (84.6°) vertex-sharing $[Fe_3(\mu_3\text{-}O)]^{7+}$ triangular units connected at Fe4. In addition, four Fe_2 edges are each bridged by an O atom (O73, O77, O83, O84) from the alkoxide arms of two $teaH^{2-}$ groups that are N,O,O-chelating on Fe2 and Fe4. The non-protonated (i.e., O^{2-}) nature of O3 and O4 were confirmed by BVS calculations (Table S4). The peripheral ligation is completed by three chelating pic^- and four *syn,syn* μ-pivalate groups. As for **1**, there are intermolecular hydrogen-bonding contacts between adjacent molecules involving an unbound $teaH^{2-}$ alcohol arm (O87) and an unbound O11 of a pic-chelate (O11···O87 = 2.741(5) Å), but unlike **1** these just form hydrogen-bonded dimers.

The core topology of **3** is unprecedented in Fe/O cluster chemistry. In fact, there are only a handful of clusters known with an $[Fe_5(\mu_3\text{-}O)_2]^{11+}$ core: $[Fe_5O_2(OMe)(bta)(btaH)(MeOH)_5Cl_5]$ (bta = benzotriazole) (**4**) [67], $[Fe_5O_2(OH)_2L_2(py)_2(H_2O)]$ (H_5L = pyrazole-expanded EDTA) (**5**) [68], $[Fe_5O_2(L')_2(O_2CPh)_7]$ (HL′ = 3-amino-1-propanol or 2-(hydroxymethyl)piperidine) (**6**) [69], $[Fe_5O_2(OH)(O_2CMe)_5(hmbp)_3](ClO_4)_2$ (hmbpH = 6-hydroxymethyl-2,2′– bipyridine) (**7**) [64], and $[Fe_5O_2(O_2CPh)_7(edte)(H_2O)]$ (H_4edte = N,N,N′,N′-tetrakis(2-hydroxyethyl)ethylenediamine) (**8**) [70]. The Fe_5 topology of **4** and **5** is an Fe-centered elongated-tetrahedron, whereas that of **7** and **8** is a butterfly unit with an additional Fe atom attached to the top. Like **3**, the core of **6** consists of two vertex-sharing $[Fe_3(\mu_3\text{-}O)]^{7+}$ triangles, but with an overall different structure with the two Fe_3 triangles nearly coplanar (dihedral angle = 23.5°).

3.3. Magnetochemistry

Solid-state, variable-temperature dc magnetic susceptibility data in the 5.0–300 K range were collected in a 1 kG (0.1 T) dc field on crushed microcrystalline samples of vacuum-dried **1**·MeCN, **2**·MeCN, and **3**·MeCN restrained in eicosane to prevent torquing. The obtained data are plotted as $\chi_M T$ versus T in Fig. 3.

The $\chi_M T$ versus T plots for **1**·MeCN and **2**·MeCN are nearly superimposable, supporting the conclusion above that they are near-isostructural except for the acetate versus benzoate difference. For this reason, we will only discuss the properties of **1** below, for which the crystal structure was obtained. For **1**, $\chi_M T$ decreases from 9.75 cm^3 K mol^{-1} at 300 K to a minimum of 9.57 cm^3 K mol^{-1} at 230 K, and then increases to a maximum of 14.60 cm^3 K mol^{-1} at 11 K before a slight drop to 14.14 cm^3 K mol^{-1} at 5.0 K. The 300 K value is much less than the spin-only value (g = 2) of 26.25 cm^3 K mol^{-1} expected for six non-interacting Fe^{III} ions, indicating antiferromagnetic (**AF**) interactions, as expected for oxo-bridged high-spin Fe^{III}. The 11 K peak value suggests a spin S = 5 ground state spin (15.00 cm^3 K mol^{-1} for g = 2) for **1**·MeCN (and **2**·MeCN). The small decrease below 11 K is likely due to ZFS splitting, Zeeman effects, and weak intermolecular interactions.

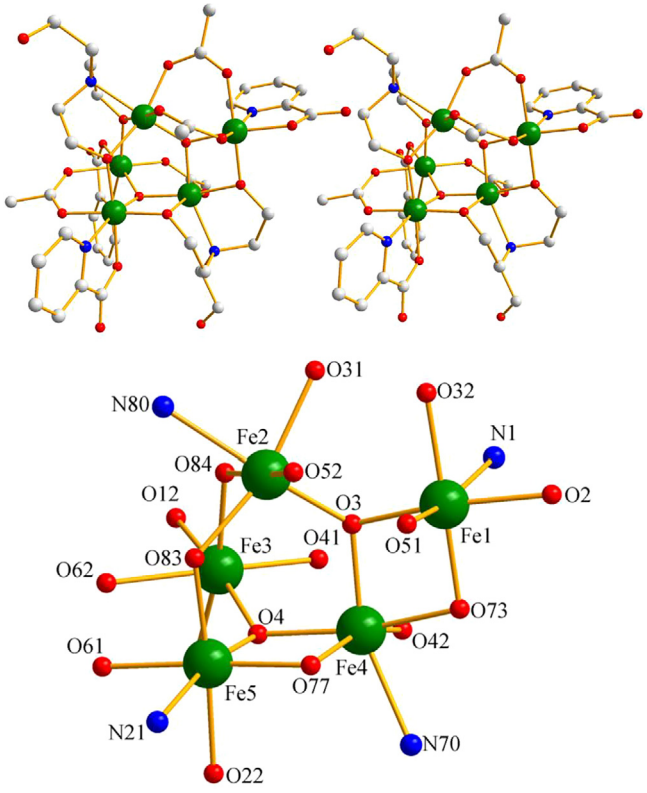

Fig. 2. A stereopair of the complete structure of complex **3**, and its labeled core; pivalate Me groups and all H atoms have been omitted for clarity. Color code: Fe, green; O, red; N, blue; C, gray. (Color online.)

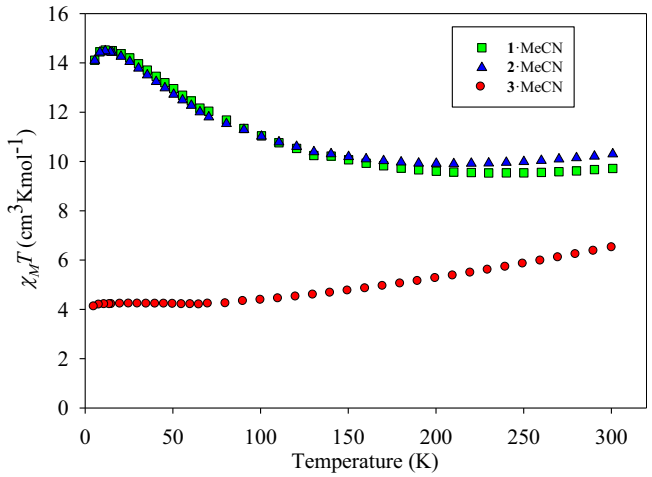

Fig. 3. $\chi_M T$ vs T plots for **1**·MeCN, **2**·MeCN, and **3**·MeCN in a 1 kG (0.1 T) dc field.

For **3**·MeCN, $\chi_M T$ steadily decreases from 6.50 cm^3 K mol^{-1} at 300 K to 4.19 cm^3 K mol^{-1} at 65 K, and then stays essentially constant, decreasing slightly below 8.0 K to 4.10 cm^3 K mol^{-1} at 5.0 K. The 300 K value is again much less than that for five non-interacting Fe^{III} ions (21.87 cm^3 K mol^{-1}) indicating strong **AF** interactions, and the 4.19 cm^3 K mol^{-1} plateau value at low T indicates an $S = {}^5/_2$ ground state.

To confirm the above ground state spin estimates for **1**·MeCN and **3**·MeCN, variable–field (H) and –temperature magnetization (M) data were collected in the 0.1–7 T and 1.8–10 K ranges, and the data are plotted in Fig. 4 as reduced magnetization ($M/N\mu_B$) versus H/T, where N is Avogadro's number and μ_B is the Bohr magneton. The saturation values at the highest fields and lowest temperatures are 9.76 and 4.85, respectively, supporting $S = 5$ and $S = 5/2$ ground state, with g slightly less than 2. The data were fit, using the program *MAGNET* [71], by diagonalization of the spin Hamiltonian matrix assuming only the ground state is populated, incorporating axial anisotropy ($D\hat{S}_z^2$) and Zeeman terms, and employing a full powder-average. The corresponding spin Hamiltonian is given by Eq. (4), where $\hat{S}_z$ is the z-axis spin operator, g is the electronic g

$$\mathscr{H} = D\hat{S}_z^2 + g\mu_B\mu_0\hat{S}\cdot H \quad (4)$$

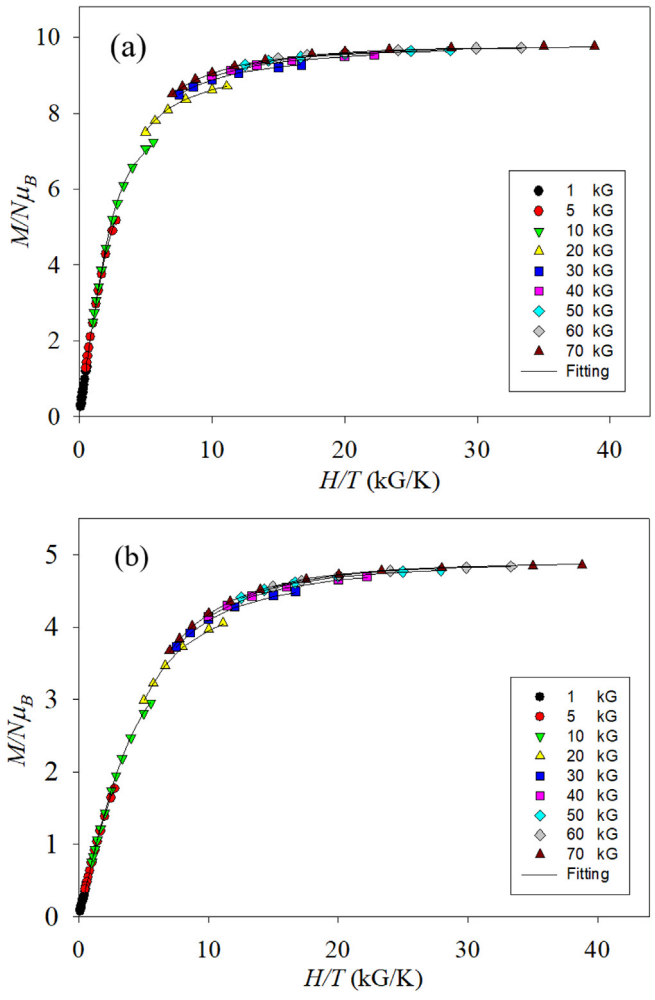

Fig. 4. Plots of reduced magnetization ($M/N\mu_B$) vs H/T data for (a) **1**·MeCN (top) and (b) **3**·MeCN at applied dc fields of 0.1–7.0 T in the 1.8–10 K temperature range. The solid lines are the fit of the data; see the text for the fit parameters.

factor, and μ_0 is the vacuum permeability; the last term is the Zeeman energy associated with an applied magnetic field. The obtained fits are shown as the solid lines in Fig. 4 and were obtained with $S = 5$, $D = -0.18(2)$ cm^{-1}, and $g = 1.96(1)$ for **1**·MeCN, and $S = {}^5/_2$, $D = -0.51(2)$ cm^{-1}, and $g = 1.96(1)$ for **3**·MeCN. Comparable quality fits were also obtained with positive D values: $S = 5$, $D = +0.27(1)$ cm^{-1}, and $g = 1.97(1)$ for **1**·MeCN, and $S = {}^5/_2$, $D = +0.63(1)$ cm^{-1}, and $g = 1.97(1)$ for **3**·MeCN. The fits are visible in the g versus D error surfaces in Figs. S3 and S4. An independent determination of the sign and magnitude of the D values was obtained from DFT calculations; these revealed that D for both **1**·MeCN and **3**·MeCN are negative, with values of $D = -0.22$ cm^{-1} and $D = -0.52$ cm^{-1}, respectively, in satisfying agreement with the results of the reduced magnetization fits.

To rule out the possibility that the dc field in the above studies was leading to complications and erroneous conclusions, an independent assessment of the ground states was obtained from ac susceptibility data obtained in zero dc field and a 3.5 G ac field. For **1**·MeCN, the ac in-phase (χ'_M) signal as $\chi'_M T$ versus T in the 1.8–15.0 K range (Fig. S1) shows a near-plateau value of ~14.5 cm^3 K mol^{-1} down to ~6 K and then drops slightly, probably due to weak intermolecular interactions. The plateau indicates a well isolated ground state, and its value indicates $S = 5$ with g ~1.97, confirming the results from the dc magnetization fit. Similarly for **3**·MeCN, which shows a near-plateau value of ~4.2 cm^3 K mol^{-1} down to ~6 K and then drops slightly, again indicating a well-isolated ground state with $S = {}^5/_2$ and $g \sim 1.96$, as found from the dc magnetization fit. Both complexes exhibited no out-of-phase (χ''_M) ac signal (Figs. S1 and S2)

3.4. Rationalization of ground state spins

It is important to understand why and how a polynuclear cluster has a particular ground state spin value. For **1** and **3**, all the exchange couplings are likely to be **AF**, and so the non-zero ground states are clearly due to spin frustration effects within the multiple Fe_3 triangular subunits. Spin frustration is here defined in the way most useful to molecular chemists, i.e., competing exchange interactions of comparable magnitude that prevent (frustrate) the preferred spin alignments. To rationalize the ground states, we thus need to determine the various exchange couplings in order to identify the relative spin alignments at the metal ions and any spin-frustrated pathways. The obvious way is to fit the experimental $\chi_M T$ versus T data but, as we have shown elsewhere, with a significant number of symmetry-inequivalent J_{ij} couplings it is possible to obtain excellent fits that are nevertheless unrelated to 'reality' [72]. The best solution to this problem is to use input values for the fit that are already good estimates for the actual J_{ij} couplings, and in the present work we have obtained these in two ways, from the use of a magnetostructural correlation (MSC) and from DFT calculations.

The MSC was formulated specifically for Fe^{III}/O clusters and allows a predicted J_{ij} to be obtained for each Fe_2 pair using its

Table 2
J_{ij} values[a] for **1** from MSC, DFT, and data fit.[b]

J_{ij}	J_{MSC}	J_{DFT}	J_{EXP}
J_{12}	−36.8	−37.2	−40.8
$J_{12'}$	−34.4	−36.9	−38.0
$J_{11'}$	−8.4	+6.6	−11.0
J_{13}	−16.5	−14.5	−12.7
J_{23}	−12.6	−12.9	−11.2
$J_{1'3}$	−10.3	−10.1	−11.4

[a] cm^{-1}.
[b] Fit of experimental $\chi_M T$ vs T data.

bridging Fe–O bond lengths and Fe–O–Fe angles [72]. For **1**, the resulting J_{MSC} are summarized in Table 2, together with the J_{DFT} obtained from a broken-symmetry DFT calculation using the hybrid version of the Perdew–Burke–Ernzerhof (PBEh) functional. The MSC predicts all J_{MSC} to be **AF** confirming that spin frustration effects should be operative within each Fe_3 triangular subunit. With one exception, the MSC and DFT values are satisfyingly similar, the exception being for the Fe1···Fe1′ interaction, where they predict weakly **AF** and weakly **F** interactions, respectively. The reason for this difference is not clear but since this interaction is completely frustrated by the stronger interactions around it (vide infra), we cannot deduce from the available data in the present work whether it is really **AF** or **F**, since both possibilities would yield the same magnetic results discussed below. Certainly weak **F** coupling between Fe^{III} centers is very rare but not unknown, having been seen in a few bis-oxo- [73] and bis-1,1-azido-bridged [74] complexes. For **3**, the obtained J_{MSC} and J_{DFT} values using the PBEh functional (Table 3) are now all **AF** and again in satisfying agreement.

The diagrammatic structure of **1** is shown in Fig. 5a with the MSC-predicted J_{MSC} values indicated for each Fe_2 pair. The two edge-fused Fe_3 triangles in the central butterfly unit each possess two strong (−34.4, −36.8 cm^{-1}) and one weak (−8.4 cm^{-1}) competing **AF** couplings. Thus, the weak $J_{11'}$ is completely frustrated and the spin alignments are determined by the strong couplings, giving a classical "spin-up, spin-down" pattern corresponding to $m_s = \pm^5/_2$ *z*-components of spin. As a result, the spin vectors at Fe1 and Fe1′ are forced to be parallel, and this same situation would prevail for a weakly **F** $J_{11'}$, as predicted by the DFT calculation. For Fe3 and Fe3′, they each interact with three Fe atoms with comparable **AF** J_{ij} values but the two interactions with the two parallel Fe1/Fe1′ spins should overcome the one interaction with Fe2, so that the Fe2Fe3 interaction is frustrated and the spins of Fe3 and Fe3′ are locked parallel to each other. The predicted ground state of **1** is then $S = 10 - 5 = 5$, in agreement with the experimental value. Using the J_{DFT} values instead would lead to the same predicted spin alignments and ground state. An $S = 5$ ground state was also found for another complex with a similar Fe_6 topology as **1** but different ligation [64].

The diagrammatic structure of **3** with J_{MSC} values (Fig. 5b) reveals that all Fe_3 triangular subunits possess two strong (−28.2 to −35.8 cm^{-1}) and one weak (−5.4 to −9.7 cm^{-1}) interactions except for the Fe2Fe3Fe5 triangle, which has two similarly weak J_{23} (−9.7 cm^{-1}) and J_{25} (−11.3 cm^{-1}) interactions consistent with their similar alkoxide bridging ligands. Nevertheless, the spin alignments are dominated by the strong interactions, frustrating the interactions in red and giving the spin alignments shown. The topology of the Fe_5 unit means that J_{23} is competing with the strong J_{24} for alignment of the Fe2 spin and is consequently frustrated, whereas J_{25} is not competing with the strong interactions and is satisfied by the antiparallel alignment of the Fe2 and Fe5 spins forced by the latter. The ground state is thus predicted as

Table 3
J_{ij} values[a] for **3** from MSC, DFT, and data fit.[b]

J_{ij}	J_{MSC}	J_{DFT}	J_{EXP}
J_{12}	−34.5	−40.9	−33.6
J_{14}	−8.5	−5.9	−7.3
J_{24}	−32.9	−38.9	−33.2
J_{34}	−28.2	−30.0	−32.4
J_{23}	−9.7	−14.0	−11.0
J_{25}	−11.3	−13.8	−15.3
J_{35}	−35.8	−39.2	−32.0
J_{45}	−5.4	−1.4	−3.3

[a] cm^{-1}.
[b] Fit of experimental $\chi_M T$ vs *T* data.

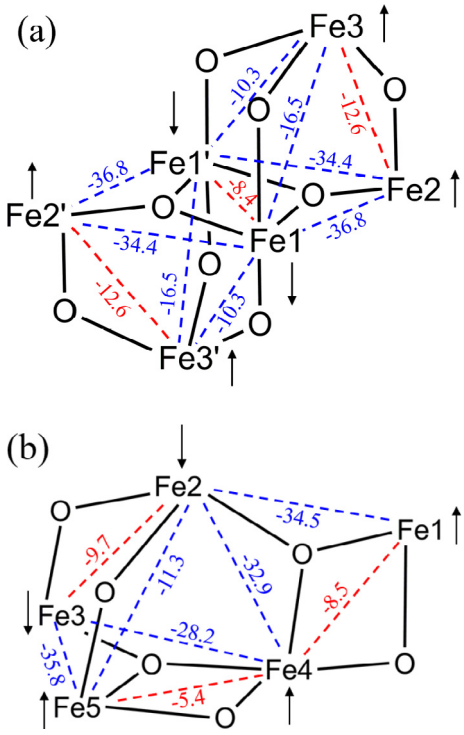

Fig. 5. Diagrammatic representation of the cores of (a) **1** and (b) **2** showing the J_{MSC} predicted values (cm^{-1}) for the various interactions, the frustrated interactions in red, and the resulting spin alignments at each Fe^{III}, which rationalize the $S = 5$ and $S = {}^5/_2$ ground states, respectively.

$S = {}^{15}/_2 - 5 = {}^5/_2$, rationalizing the experimental data. Again, using the J_{DFT} values would lead to the same predicted ground state spin alignments and thus would equally rationalize the experimental data.

3.5. Fit of experimental data

As stated above, an important use of J_{MSC} and/or J_{DFT} data is to provide input values for fits of high nuclearity Fe_x complexes to minimize problems from over-parameterization, especially for complexes with no virtual symmetry to decrease the number of independent J_{ij} parameters. Thus, for centrosymmetric **1**·MeCN the dc $\chi_M T$ versus *T* data in the 11.0–300 K range (to avoid the lower-*T* drop due to intermolecular interactions and/or ZFS) were fit using the program PHI [75] with the six J_{MSC} as input values, *g* fixed at 1.96, and a TIP term of 100×10^{-6} cm^3 mol^{-1} per Fe. An excellent fit was obtained (solid line in Fig. 6) with J_{EXP} values only slightly different from the J_{MSC} inputs (Table 2). For **3**·MeCN, there is no crystallographic or even virtual symmetry to help, and thus eight unique J_{ij} values. Nevertheless, using the J_{MSC} as inputs, *g* fixed at 1.96, and TIP as for **1**·MeCN, an excellent fit for the 11.0–300 K data was obtained (solid line in Fig. 6) with the J_{EXP} values in Table 3. The fit parameters for **1**·MeCN reveal the first and second excited states are both $S = 4$ at energies of 46.2 and 92.5 cm^{-1}, respectively, above the $S = 5$ ground state. For **3**·MeCN, the first and second excited states are $S = {}^3/_2$ and $S = {}^7/_2$ at energies of 101.8 and 151.4 cm^{-1}, respectively, above the $S = {}^5/_2$ ground state.

4. Conclusions

The use of a mixed-chelate reaction system with $[Fe_3O(O_2CR)_6(H_2O)_3]^+$ has yielded three new clusters **1**, **2**, and **3** of two structural types, Fe_6 and Fe_5, whose cores consist of fused Fe_3 triangular

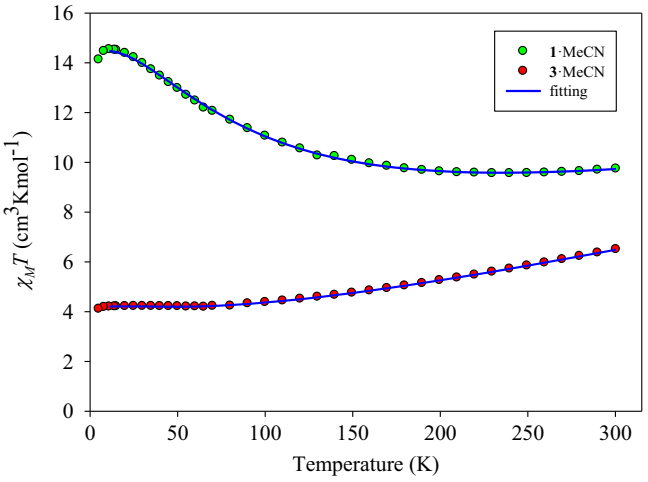

Fig. 6. Experimental $\chi_M T$ vs T for **1**·MeCN and **3**·MeCN. The solid lines are the fits of the data. See Tables 2 and 3 for the fit parameters.

subunits and thus experience spin frustration effects from competing **AF** interactions yielding $S = 5$ ground states for **1**/**2** and $S = {}^5/_2$ for **3**. The cohesive analysis of the magnetic properties using a combination of DFT calculations, use of a MSC, and fit of experimental data emphasizes the power of such a multi-component approach to rationalize ground states and extract credible J_{ij} values.

Acknowledgments

This work was supported by the U.S. Department of Energy, Office of Science, Office of Basic Energy Sciences, as part of the Computational Chemical Sciences Program under Award #DE-SC0018331.

Appendix A. . Supplementary data

CCDC 1950286 and 1950285 contains the supplementary crystallographic data for **1**·4MeCN and **3**·½teaH$_3$·2MeCN, respectively. These data can be obtained free of charge via http://www.ccdc.cam.ac.uk/conts/retrieving.html, or from the Cambridge Crystallographic Data Centre, 12 Union Road, Cambridge CB2 1EZ, UK; fax: (+44) 1223-336-033; or e-mail: deposit@ccdc.cam.ac.uk. Supplementary data to this article can be found online at https://doi.org/10.1016/j.poly.2019.114182.

References

[1] S. Herold, S.J. Lippard, J. Am. Chem. Soc. 119 (1997) 145.
[2] D. Lee, S.J. Lippard, J. Am. Chem. Soc. 120 (1998) 12153.
[3] M. Kodera, M. Itoh, K. Kano, T. Funabiki, M. Reglier, Angew. Chem. Int. Ed. 44 (2005) 7104.
[4] G. Xue, D. Wang, R. De Hont, A.T. Fiedler, X. Shan, E. Münck, L. Que, Proc. Natl. Acad. Sci. U. S. A. 104 (2007) 20713.
[5] M. Costas, J.U. Rohde, A. Stubna, R.Y.N. Ho, L. Quaroni, E. Münck, L. Que, J. Am. Chem. Soc. 123 (2001) 12931.
[6] M. Sankaralingam, M. Palaniandavar, Polyhedron 67 (2014) 171.
[7] H. Arii, S. Nagatomo, T. Kitagawa, T. Miwa, K. Jitsukawa, H. Einaga, H. Masuda, J. Inorg. Biochem. 82 (2000) 153.
[8] T.J. Mizoguchi, J. Kuzelka, B. Spingler, J.L. DuBois, R.M. Davydov, B. Hedman, K. O. Hodgson, S.J. Lippard, Inorg. Chem. 40 (2001) 4662.
[9] C. He, Y. Mishina, Curr. Opin. Chem. Biol. 8 (2004) 201.
[10] S. Ménage, Y. Zang, M.P. Hendrich, L. Que, J. Am. Chem. Soc. 114 (1992) 7786.
[11] X. Zhang, H. Furutachi, S. Fujinami, S. Nagatomo, Y. Maeda, Y. Watanabe, T. Kitagawa, M. Suzuki, J. Am. Chem. Soc. 127 (2005) 826.
[12] L. Que, Acc. Chem. Res. 40 (2007) 493.
[13] E.Y. Tshuva, S.J. Lippard, Chem. Rev. 104 (2004) 987.
[14] D. Foguet-Albiol, K.A. Abboud, G. Christou, Chem. Commun. 2 (2005) 4282.
[15] J.K. McCusker, E.A. Schmiit, P.M. Hagen, D.N. Hendrickson, J.B. Vincent, M.L. Mino, K. Shin, D.A.K. Coggin, G. Christou, J.C. Huffman, J. Am. Chem. Soc. 113 (1991) 3012.
[16] D. Gatteschi, A. Caneschi, R. Sessoli, A. Cornia, Chem. Soc. Rev. 25 (1996) 101.
[17] O. Kahn, Chem. Phys. Lett. 265 (1997) 109.
[18] B.P. Murch, P.D. Boyle, L. Que, J. Am. Chem. Soc. 107 (1985) 6728.
[19] A.N. Mansour, C. Thompson, E.C. Theil, N.D. Chasteen, D.E. Sayers, J. Biol. Chem. 260 (1985) 7975.
[20] Q.T. Islam, D.E. Sayers, S.M. Gorun, E.C. Theil, J. Inorg. Biochem. 36 (1989) 51.
[21] K.L. Taft, G.C. Papaefthymiou, S.J. Lippard, Inorg. Chem. 33 (1994) 1510.
[22] R.J. Lachicotte, K.S. Hagen, Inorg. Chim. Acta 263 (1997) 407.
[23] B. Xu, N. Chasteen, J. Biol. Chem. 266 (1991) 19965.
[24] E. Theil, Annu. Rev. Biochem. 56 (1987) 289.
[25] E.C. Theil, M. Matzapetakis, X. Liu, J. Biol. Inorg. Chem. 11 (2006) 803.
[26] G.C. Ford, P.M. Harrison, D.W. Rice, J.M.A. Smith, A. Treffry, J.L. White, J. Yariv, Philos. Trans. R. Soc. London, Ser. B 304 (1984) 551.
[27] T. Taguchi, M.S. Thompson, K.A. Abboud, G. Christou, Dalton Trans. 39 (2010) 9131.
[28] I.A. Gass, C.J. Milios, M. Evangelisti, S.L. Heath, D. Collison, S. Parsons, E.K. Brechin, Polyhedron 26 (2007) 1835.
[29] D. Gatteschi, R. Sessoli, A. Cornia, Chem. Commun. (2000) 725.
[30] C. Sangregorio, T. Ohm, C. Paulsen, R. Sessoli, D. Gatteschi, Phys. Rev. Lett. 78 (1997) 4645.
[31] G. Christou, D. Gatteschi, D.N. Hendrickson, R. Sessoli, MRS Bull. 25 (2000) 66.
[32] A.K. Powell, S.L. Heath, D. Gatteschi, L. Pardi, R. Sessoli, G. Spina, F. Del Giallo, F. Pieralli, J. Am. Chem. Soc. 117 (1995) 2491.
[33] C. Cañada-Vilalta, T.A. O'Brien, E.K. Brechin, M. Pink, E.R. Davidson, G. Christou, Inorg. Chem. 43 (2004) 5505.
[34] R. Bagai, G. Christou, Chem. Soc. Rev. 38 (2009) 1011.
[35] D. Gatteschi, M. Fittipaldi, C. Sangregorio, L. Sorace, Angew. Chem. Int. Ed. 51 (2012) 4792.
[36] P. King, T.C. Stamatatos, K.A. Abboud, G. Christou, Angew. Chem. Int. Ed. 45 (2006) 7379.
[37] O. Botezat, J. Van Leusen, P. Kögerler, S.G. Baca, Inorg. Chem. 57 (2018) 7904.
[38] M.D. Godbole, O. Roubeau, A.M. Mills, H. Kooijman, A.L. Spek, E. Bouwman, Inorg. Chem. 45 (2006) 6713.
[39] K. Graham, A. Darwish, A. Ferguson, S. Parsons, M. Murrie, Polyhedron 28 (2009) 1830.
[40] M. Murugesu, K.A. Abboud, G. Christou, J. Chem. Soc., Dalton. Trans. 3 (2003) 4552.
[41] A.K. Boudalis, Y. Sanakis, F. Dahan, M. Hendrich, J.P. Tuchagues, Inorg. Chem. 45 (2006) 443.
[42] M.W. Wemple, D.K. Coggin, J.B. Vincent, J.K. McCusker, W.E. Streib, J.C. Huffman, D.N. Hendrickson, G. Christou, J. Chem. Soc., Dalton. Trans. 4 (1998) 719.
[43] W. Schmitt, L. Zhang, C.E. Anson, A.K. Powell, Dalton Trans. 39 (2010) 10279.
[44] S.J. Liu, S. De Han, J.M. Jia, L. Xue, Y. Cui, S.M. Zhang, Z. Chang, Cryst. Eng. Comm. 16 (2014) 5212.
[45] O. Botezat, J. Van Leusen, V.Ch. Kravtsov, A. Ellern, P. Kögerler, S.G. Baca, Dalton Trans. 44 (2015) 20753.
[46] T. Liu, Y.-J. Zhang, Z.-M. Wang, S. Gao, J. Am. Chem. Soc. 130 (2008) 10500.
[47] L.F. Jones, P. Jensen, B. Moubaraki, K.J. Berry, J.F. Boas, J.R. Pilbrow, K.S. Murray, J. Mater. Chem. 16 (2006) 2690.
[48] A.M. Ako, O. Waldmann, V. Mereacre, F. Klöwer, I.J. Hewitt, C.E. Anson, H.U. Güdel, A.K. Powell, Inorg. Chem. 46 (2007) 756.
[49] A.M. Bond, R.J.H. Clark, D.G. Humphrey, P. Panayiotopoulos, B.W. Skelton, A.H. White, Dalton. Trans. 3 (1998) 1845.
[50] shelxtl2014, Bruker-AXS, Madison, WI, (2014).
[51] G.A. Bain, J.F. Berry, J. Chem. Educ. 85 (2009) 532.
[52] (a) A. Bencini, F. Totti, C.A. Daul, K. Doclo, P. Fantucci, V. Barone, Inorg. Chem. 36 (1997) 5022;
(b) E. Ruiz, A. Rodríguez-Fortea, J. Cano, S. Alvarez, P. Alemany, J. Comput. Chem. 24 (2003) 982.
[53] R. Valero, R. Costa, I. De P. R. Moreira, D.G. Truhlar, F. Illas, J. Chem. Phys. 128 (2008).
[54] P. Comba, S. Hausberg, B. Martin, J. Phys. Chem. A. 113 (2009) 6751.
[55] J.J. Phillips, J.E. Peralta, J. Chem. Theory Comput. 8 (2012) 3147.
[56] R.P. Joshi, J.J. Phillips, K.J. Mitchell, G. Christou, K.A. Jackson, J.E. Peralta (Manuscript in preparation).
[57] (a) R. Krishnan, J.S. Binkley, R. Seeger, J.A. Pople, J. Chem. Phys. 72 (1980) 650;
(b) J. Blaudeau, M.P. Mcgrath, L.A. Curtiss, L. Radom, J. Chem. Phys. 2 (1997) 5016.
[58] C. Van Wüllen, J. Phys. Chem. A. 113 (2009) 11535.
[59] M.J. Frisch et al., Gaussian 16, Revision B.01 (2016).
[60] M.R. Pederson, S.N. Khann, Phys. Rev. B 60 (1999) 9566.
[61] A.V. Postnikov, J. Kortus, M.R. Pederson, Phys. Stat. Sol. (B) 243 (2006) 2533.
[62] R. Bagai, S. Datta, A. Betancur-Rodriguez, K.A. Abboud, S. Hill, G. Christou, Inorg. Chem. 46 (2007) 4535.
[63] I.D. Brown, D. Altermatt, Acta Crystallogr., Sect: B 41 (1985) 244.
[64] R. Bagai, K.A. Abboud, G. Christou, Inorg. Chem. 46 (2007) 5567.
[65] P.S. Ammala, S.R. Batten, J.D. Cashion, C.M. Kepert, B. Moubaraki, K.S. Murray, L. Spiccia, B.O. West, Inorg. Chim. Acta 331 (2002) 90.
[66] C. Papatriantafyllopoulou, C.M. Kizas, M.J. Manos, A. Boudalis, Y. Sanakis, A.J. Tasiopoulos, Polyhedron 64 (2013) 218.
[67] J. Tabernor, L.F. Jones, S.L. Heath, M. Chris, G. Aromi, J. Ribas, E.K. Brechin, D. Collison, Dalton Trans. (2004) 975.

[68] S. Fischer, S. Demeshko, S. Dechert, F. Meyer, Z. Anorg. Allg. Chem. 638 (2012) 621.
[69] C.M. Kizas, M.J. Manos, V. Nastopoulos, A.K. Boudalis, Y. Sanakis, A.J. Tasiopoulos, Dalton Trans. 41 (2012) 1544.
[70] R. Bagai, M.R. Daniels, K.A. Abboud, G. Christou, Inorg. Chem. 47 (2008) 3318.
[71] E.R. Davidson, MAGNET, Indiana University, Bloomington, IN, 1999.
[72] K.J. Mitchell, K.A. Abboud, G. Christou, Inorg. Chem. 55 (2016) 6597.
[73] B.S. Snyder, G.S. Patterson, A.J. Abrahamson, R.H. Holm, J. Am. Chem. Soc. 111 (1989) 5214.
[74] (a) G. De Munno, T. Poerio, G. Viau, M. Julve, F. Lloret, Angew. Chem. Int. Ed. Engl. 36 (1997) 1459;
(b) K.R. Reddy, M.V. Rajasekharan, J.-P. Tuchagues, Inorg. Chem. 37 (1998) 5978;
(c) S. Naiya, M.G.B. Drew, C. Diaz, J. Ribas, A. Ghosh, Eur. J. Inorg. Chem. (2011) 4993.
[75] N.F. Chilton, R.P. Anderson, L.D. Turner, A. Soncini, K.S. Murray, J. Comput. Chem. 34 (2013) 1164.